# UC San Diego

## UC San Diego Previously Published Works


### Title

Structural basis for selective inhibition of human PKG Iα by the balanol-like compound N46


### Permalink

https://escholarship.org/uc/item/3096c18d



### Journal

Journal of Biological Chemistry, 293(28)

### ISSN

0021-9258



### Authors

Qin, Liying
Sankaran, Banumathi
Aminzai, Sahar
et al.



### Publication Date

2018-07-01

### DOI

10.1074/jbc.ra118.002427

Peer reviewed



eScholarship.org Powered by the California Digital Library
University of California

JBC Papers in Press. Published on May 16, 2018 as Manuscript RA118.002427
The latest version is at http://www.jbc.org/cgi/doi/10.1074/jbc.RA118.002427

# Structural basis for selective inhibition of human PKG Iα by the balanol-like compound N46

**Liying Qin[1], Banumathi Sankaran[2], Sahar Aminzai[3], Darren E. Casteel[3,*], Choel Kim[1,4,*]**

From the [1]Verna and Marrs McLean Department of Biochemistry and Molecular Biology, Baylor College of Medicine, Houston TX 77030; [2]Berkeley Center for Structural Biology, Lawrence Berkeley National Laboratory, Berkeley CA 94720; [3]Department of Medicine, University of California, San Diego, La Jolla CA92093; [4]Department of Pharmacology and Chemical Biology, Baylor College of Medicine, Houston TX77030

Running Title: *N46 Specificity for PKG Iα*

*To whom correspondence should be addressed: Darren E. Casteel: Department of Medicine, University of California, San Diego, La Jolla CA92093; Tel: (858)534-8806; Email: dcasteel@ucsd.edu; Choel Kim, Department of Pharmacology and Chemical Biology, Baylor College of Medicine, Houston TX77030; Tel: 713-798-8411; Email: ckim@bcm.edu

**Keywords:** cyclic GMP; cGMP; protein kinase G; PKG; crystal structure; drug design; kinase inhibitor; inhibitor specificity; ATP competitive inhibitor; protein-ligand complex; nonopioid analgesics

## ABSTRACT

Activation of PKG Iα in nociceptive neurons induces a long-term hyperexcitability that causes chronic pain. Recently, a derivative of the fungal metabolite balanol, N46, has been reported to inhibit PKG Iα with high potency and selectivity and attenuates thermal hyperalgesia and osteoarthritic pain. Here, we determined co-crystal structures of the PKG Iα C-domain and cAMP-dependent protein kinase (PKA) Cα, each bound with N46, at 1.98 Å and 2.65 Å, respectively. N46 binds the active site with its external phenyl ring specifically interacting with the glycine-rich loop and the αC helix. Phe371 at the PKG Iα glycine-rich loop is oriented parallel to the phenyl ring of N46, forming a strong π-stacking interaction, while the analogous Phe54 in PKA Cα rotates 30º and forms a weaker interaction. Structural comparison revealed that steric hindrance between the preceding Ser53 and the propoxy group of the phenyl ring may explain the weaker interaction with PKA Cα. The analogous Gly370 in PKG Iα, however, causes little steric hindrance with Phe371. Moreover, Ile406 on the αC helix forms a hydrophobic interaction with N46 while its counterpart in PKA, Thr88, does not. Substituting these residues in PKG Iα with those in PKA Cα increases its $IC_{50}$ values for N46 whereas replacing these residues in PKA Cα with those in PKG Iα reduces the IC50, consistent with our structural findings. In conclusion, our results explain the structural basis for N46-mediated selective inhibition of human PKG Iα and provide a starting point for structure-guided design of selective PKG Iα inhibitors.

Chronic pain is a debilitating condition that affects nearly 25 million U.S. adults (1). Opioid pain relievers (OPRs) are the most prescribed medication class in the US (2). The increasing prescription of OPRs is associated with the dramatic increase in opioid misuse, abuse, overdose, and opioid use disorder, contributing to $504 billion economic cost in US in 2015 and more than 63,600 opioid overdose deaths in 2016 (2-6). Another major category of analgesics, COX inhibitors, has long-term cardiovascular side effects (7). Therefore, a new type of non-opioid based pain reliever is in demand for effective pain management.

Reversible protein phosphorylation regulates all aspects of cell survival. Consequently, dysregulations of protein kinases are often involved in human diseases such as cancer (8), diabetes (9-11), and chronic pain (12,13). Over thirty protein kinase inhibitors have been approved by FDA in the past 23 years and the majority of them are targeting tyrosine kinases for cancer treatment (14).

Beyond its role as a central regulator of smooth muscle tone, cyclic GMP-dependent protein kinase (PKG) Iα activation in nociceptive neurons results in long-term hyperexcitability that causes chronic pain (15,16). PKG Iα is also a



Downloaded from http://www.jbc.org/ at University of California, Berkeley on November 28, 2018

crucial modulator of cortical neuronal activity in pathological pain, thus it represents a novel target for developing analgesic therapeutics (17). A recent study demonstrated that N46, a derivative of fungal metabolite balanol, inhibits PKG Iα with high potency and selectivity, resulting in the attenuation of thermal hyperalgesia and osteoarthritic pain in rats (18).

PKG Iα belongs to the AGC kinase family and consists of N-terminal regulatory (R) and C-terminal catalytic (C) domains (Figure 1A) (19,20). PKG Iα shares a large degree of sequence similarity with cAMP-dependent protein kinase (PKA). In particular, the PKG Iα C-domain shows 45% sequence identity with the PKA Cα, consistent with their similar structures. The C-domain includes small and large lobes that consist of mostly β strands and α helices, respectively. A highly acidic active site is formed between the two lobes, which binds $Mg^{2+}$, ATP, and substrates. In the absence of cGMP, activity of PKG Iα is negatively regulated by the interaction between the R and C-domains (21,22).

Three classes of small molecule PKG inhibitors have been widely used for the functional studies of PKG (23,24). The first class is the R-diastereomer of the phosphorothioate analogs of cGMP including Rp-cGMPS (25). This compound binds the R-domain and stabilizes its inactive state without causing conformational changes required for activation (26). The second class consists of small molecules that compete with ATP by directly binding the active site within the C-domain. These reagents include H-89, balanol, and KT-5823 (27-32). The third class includes peptide inhibitors that also bind the active site and prevent substrate binding. However, all of these inhibitors lack potency, specificity, and activity *in vivo*. For example, Rp-cGMPS is not potent ($Ki$= 49μM) and non-selectively inhibits other cyclic nucleotide effectors such as phosphodiesterase and PKA (23). KT-5823 also inhibits other kinases and may not inhibit PKG in intact cells (33). Despite its high potency *in vitro*, DT-2 does not inhibit PKG in platelets or in rat mesangial cells (34).

As mentioned, balanol is a potent inhibitor of PKG, but also inhibits other serine and threonine kinases such as PKA, most PKC isoforms, and $Ca^{2+}$-dependent protein kinase (30,35). To improve inhibitor selectivity for PKG Iα, a homology model of PKG Iα docked with balanol was generated based on the crystal structure of the PKA Cα:balanol complex, several amino-acid differences near their binding pockets were identified, and balanol was modified to preferentially interact with PKG Iα specific residues (18). In particular, the homology model showed that Thr88 of PKA Cα corresponds to Ile406 in PKG Iα (16). To exploit this difference, a propoxy group was added to the external phenyl ring (ring D) of the balanol derivatives to selectively interact with Ile406 of PKG Iα. While one such compound, N46, was reported to have a high selectivity and potency for PKG Iα over PKA Cα, the exact molecular basis for its improved affinity and specificity is unknown.

**Results and Discussion**

Several crystal structures have been solved for mammalian PKG I, but these are of various fragments of the R-domains (36-39). Since N46 directly targets the C-domain of PKG Iα, we first obtained an isolated C-domain that is fully active. To understand the molecular basis of N46's high selectivity for human PKG Iα, we determined co-crystal structures of N46 bound to the human PKG Iα C-domain and human PKA Cα for a direct comparison at 1.98 Å and 2.65 Å, respectively (Figure 1, Figure S1, and Table S1). The PKG Iα C:N46 complex was crystallized in the $P4_2$ space group with 1 molecule in the asymmetric unit. The molecule shows clear electron density for the bound N46 and the C-domain used for crystallization excluding the first 10 residues at the N-terminus (Figure 1B). The PKA Cα:N46 complex was crystallized in the $P3_121$ space group with one molecule in the asymmetric unit (Figure 1C and Figure S1). The final model shows clear density for the Cα-subunit except for the first 10 residues. Unlike previous PKA Cα structures, the N-terminal αA helix disengages from the catalytic core due to unusual crystal packing interactions (Figure S2). The αA helix of a neighboring symmetry mate occupies the equivalent position seen in previous structures, and provides the same set of interactions with the catalytic core.

The overall structure of the PKG Iα C:N46 complex is similar to the AMP-PNP-bound structure (Unpublished manuscript). It shows a closed conformation with the fully ordered glycine rich loop and C-terminal tail (Figure 1B). N46 binds to a pocket that extends from the hinge region to the inner surface of the αC helix and spans approximately 20 Å (Figure 2A). The pocket can be divided into three subsites according to the interaction between PKG Iα C-domain and AMP-



Downloaded from http://www.jbc.org/ at University of California, Berkeley on November 28, 2018

PNP: the adenine, the ribose, and the extended triphosphate subsites. N46 binds to all three subsites in the extended active site of the PKG Iα C-domain (Figure 2A).

The A-ring (indazole ring) binds the adenine subsite consisting of the hinge (loop between β5-αD) and hydrophobic residues from both small and large lobes (Figure 2B). Specifically, the protonated 1-N binds the backbone carbonyl of Glu439 while the unprotonated 2-N interacts with the backbone amide of Cys441 through hydrogen bonds. Additionally, the indazole ring is surrounded by several hydrophobic residues that coat the adenine subsite. These residues include Leu366, Val374, Ala388, Val422, Met438, Ile491, Val501, and Phe649.

The B-ring (pyrrolidine ring), which connects the A-ring to the C-ring, interacts with the acidic ribose subsite directly and indirectly through water molecules (Figure 2B). The ribose subsite consists of the hinge and activation loop residues. The side chains of Glu445 at the hinge and Asp502 at the activation loop form hydrogen bonds with the amine groups on either side. Two water molecules bridge the interaction with N46 at this subsite. These water molecules are located adjacent to the amide connecting the B-ring to the A-ring, bridging them to the side chains of Glu445 and Asp502 through hydrogen bonds.

The C-ring (phenyl ring) interacts with β1 and the glycine rich loop through van der Waals (VDW) contacts (Figure 2B). In particular, Val368, Gly369, and Gly370 are within 3.4-3.8 Å from the C-ring, providing VDW interactions. Since these interactions are through backbone atoms, this region does not provide any PKG selective contacts.

The D-ring (external phenyl ring) with the propoxy and methoxy groups provides two interactions that are PKG specific and may explain its high selectivity for PKG Iα over PKA Cα (Figure 2B). In designing N46, the propoxy group was added to the phenyl ring to provide a preferential interaction with Ile406 of PKG Iα over PKA Cα, which has a threonine (Thr88) at the analogous position (Figure S3) (18). However, the structure shows that the methoxy group points towards the side chain of Ile406 instead, while the propoxy group points towards the glycine-rich loop, each providing hydrophobic interactions. Additionally, the D-ring, along with the carbonyl group that connects the D-ring to the C-ring, docks to the tip of the glycine rich loop through hydrogen bonds and VDW interactions. The interconnecting carbonyl group hydrogen bonds with the backbone amide of Phe371 and uniquely forms a lone-pair-π interaction with its side chain. The D-ring and the side chain of Phe371 are off-centered, and they interact through a parallel-displaced π interaction.

The overall interactions between the PKA Cα-subunit and N46 are similar to those in the PKG Iα C:N46 complex, because most of the contact residues are highly conserved between the two kinases (Figure 3A). However, the structure shows differences that may explain a higher $IC_{50}$ value for PKA Cα-subunit.

The A-ring binds the adenine subsite and the interactions in this region are essentially the same as in PKG Iα. These include hydrogen bonds between A-ring and the backbone atoms of Glu121 and Val123 at the hinge and VDW contacts with a hydrophobic pocket consisting of Leu49, Val57, A70, Val104, Met120, Leu173, and Phe327 (Figure 3B). Tyr122 at the hinge region provides an additional hydrophobic contact unseen in PKG Iα because Tyr122 replaces Ala440 of PKG Iα. While the B-ring similarly docks onto the ribose subsite, its amine group interacts only with the hinge residue Glu127 through a hydrogen bond, not with the activation loop residue Asp184 (Figure 3B). Unlike Asp502 of PKG I that forms a hydrogen bond with N46 (Figure 2B), the side chain of Asp184 points away and no longer interacts with N46 in PKA. The C-ring similarly docks to β1 and the glycine rich loop and interacts with the backbone atoms of Thr51, Gly52, and Ser53.

The D-ring interacts less strongly with PKA Cα compared to PKG Iα because of two PKA specific residues, Phe54 and Thr88 (Figure 3B). The structure shows that the side chain of Phe54 at the tip of the glycine rich loop rotates approximately 30º and provides a weaker T-shaped π interaction with the D-ring. Due to this rotation, the interconnecting carbonyl no longer forms a lone-pair-π interaction with the aromatic Phe54. In addition, the side chain of Thr88 of the αC helix is smaller and less hydrophobic than that of Ile406 of PKG Iα, thus provides much weaker hydrophobic interaction with the methoxy group (3.7 Å) (Figure 3B). The structural alignment with the PKG Iα C:N46 complex suggests that a steric clash between the side chain of the preceding residue S53 and the propoxy moiety causes the rotation of the Phe54 side chain. As seen in Figure S3, N46 moves away slightly from the active site due to the steric clash.



Downloaded from http://www.jbc.org/ at University of California, Berkeley on November 28, 2018

This allows more room between the D-ring and the glycine rich loop, causing the rotation of the F54 side chain.

The reported inhibition constant of balanol for PKA Cα is 1.6 nM while N46 inhibits PKA with an $IC_{50}$ of 1.0 μM, showing an over 600-fold increase (18). Comparing the PKA Cα:N46 complex with the PKA Cα:Balanol complex reveals that this reduction is mostly due to loss of hydrogen bonds (Figure 4). The PKA Cα:Balanol complex shows 12 non-solvent mediated hydrogen bonds and large numbers of VWD interactions between the extended active site and balanol. The PKA Cα:N46 complex shows that, while the most of the VDW contacts are preserved, N46 forms only 6 direct hydrogen bonds because of the modifications on the C and D rings.

Substituting the phenol of balanol (Ring a in Figure 4A) with the indazole ring of N46 (Ring A in Figure 4B) does not reduce the number of hydrogen bonds and VDW contacts with the adenine subsite (Figure 4). In the PKA:Balanol complex, the phenol forms hydrogen bonds with the same backbone atoms of Glu121 and Val123 at the hinge region (Figure 4A) as the indazole does. However, replacing a more puckered azepane ring of balanol (Ring b in Figure 4A) with a less puckered pyrrolidine of N46 (Ring B in Figure 4B) results in one additional hydrogen bond at the ribose subsite. The puckered azepane ring interacts mainly with a conserved catalytic loop residue, Glu170, through its backbone (Figure 4A). In the PKA:N46 complex, the less puckered pyrrolidine ring brings its amine group within a hydrogen bonding distance of the Glu127 side chain, forming a new hydrogen bonds (Figure 4B).

Removing two hydroxyl groups from the c-ring of balanol (Figure 4A) disrupts all four hydrogen bonds with the triphosphate subsite. In the PKA Cα:balanol complex, two hydroxyl groups on the c-ring interact with Gly55, Lys72, and Asp184 through 4 hydrogen bonds. In major contrast, the C-ring of N46 (Figure 4B) no longer binds these residues and interacts with the glycine rich loop through VDW contacts.

Lastly, substituting a carboxyl group and a hydroxyl group on the d-ring of balanol (Figure 4A) with a bulky and hydrophobic propoxy group and a fluorine atom, respectively, (Ring D of N46, Figure 4B) significantly weakens the interaction with the glycine rich loop and the αC helix. In the PKA:balanol complex, the carboxyl group on the d-ring forms strong hydrogen bonds with both the side chain and backbone of Ser53 at the glycine rich loop while the 3-hydroxyl group binds the side chains of Glu91 and Lys72 through hydrogen bonds. Additionally, the d-ring is oriented parallel to the side chain of Phe54, allowing a parallel π-stacking interaction between them as well as a lone-pair - π interaction between the carbonyl group and Phe54. None of these interactions is preserved in the PKA:N46 complex although a new hydrogen bond forms between the propoxy group and the backbone amide of Ser53.

We noticed that the side chain of Phe54 remains parallel to the d-ring when bound to balanol and rotates when bound to N46 (35). The balanol-bound PKA structure shows that this is because balanol binds deeper into the pocket, allowing a parallel π-stacking interaction with Phe54 (Figure S4A). In contrast, N46 cannot bind as deep due to its bulky methoxy group, resulting in enough space between the D-ring and Phe54, which allows Phe54 to rotate to provide VDW contact with the D-ring (Figure S4B).

To test the molecular basis for N46's PKG Iα selective inhibition over PKA, we mutated the unique contact residues in PKG Iα to those in PKA and vice versa. Specifically, for PKG Iα, we mutated G370 and I406 to the corresponding residues in PKA Cα (i.e. G370S and I406T). We also mutated these two PKA Cαα residues into the corresponding PKG Iα residues (S53G and T88I). For PKG Iα, we generated two single mutants (G370S and I406T) and a double mutant (G370S/I406T). For PKA Cα, we only generated a double mutant (S53G/T88I). We then measured $IC_{50}$ values using *in vitro* kinase assays (Figure 5). N46 showed an $IC_{50}$ of 43 nM for wild-type PKG Iα, whereas it inhibited PKA Cα with an $IC_{50}$ of 1030 nM, showing an ~24-fold difference in selectivity. The PKG Iα single mutants were inhibited with higher $IC_{50}$ values of 90 nM and 142 nM for G370S and I406T, respectively. The double mutant PKG Iα showed an $IC_{50}$ value of 301 nM, demonstrating a synergistic effect of the two mutations. In contrast, the PKA Cα double mutant showed an $IC_{50}$ of 552 nM, which is almost half that seen in wild-type Cα. The higher $IC_{50}$ values seen in the PKG Iα mutants and the lower value of the PKA Cα double mutant compared to their respective wild type are consistent with our structural findings.

Despite lack of data on inhibition constants of N46 for other kinases, our model of a PKCα isoform (PDB ID: 3IW4) docked with N46 suggests



Downloaded from http://www.jbc.org/ at University of California, Berkeley on November 28, 2018

that N46 is a poor inhibitor for the PKCα isoform (Figure S5) (40). The model shows that the tip of the glycine rich loop curls in toward the active site and clashes with the C-ring. In particular, F350 at the glycine rich loop occupies the part of the pocket that the C-ring binds, suggesting that N46 would interact poorly with PKCα. Consistent with the model, Sung *et al* reported that at 0.75 μM of N46, PKCδ had 68% residual activity while PKG Iα was completely inhibited with 0% residual activity (18).

Our structural and biochemical data suggest new strategies for generating N46 derivatives with higher selectivity for PKG Iα over PKA Cα. Amino acid sequences at the hinge region and β7 that make up the left edge and the base of the adenine pocket are different in PKG Iα compared to PKA Cα. PKG Iα has Ala-Cys-Leu (residues 440-442) at the hinge whereas PKA has Tyr-Val-Pro (residues 122-124) (Figure S6). This causes PKG Iα to have a wider adenine pocket compared to PKA Cα-subunit (Figure 6). Additionally, at the base of the adenine pocket, PKG Iα has an isoleucine (I491 at β7) replacing a leucine (L173) of PKA Cα, providing a slightly deeper pocket. Thus, to improve selectivity for PKG Iα, bulkier heterocyclic rings could be engineered in N46 to fill this unique pocket. Also, a reactive group can be placed here to covalently link to the conserved Cys441 since PKA lacks a cysteine residue at the analogous position (Figure S6). During the initial design of N46, the propoxy group was added to increase its interaction with Ile406 at the αC helix. However, our structures revealed that this group points to an opposite direction (toward the glycine rich loop) and interacts with Gly370 instead. Thus, it may be possible to add an additional ethyl or propyl group here to improve interaction with PKG Iα. This modification should cause steric hindrance with Ser53 of PKA at the glycine rich loop while providing additional nonpolar interactions with Gly370 in PKG Iα. In conclusion, our structural and biochemical data in part explain N46's selectivity for PKG Iα and provides a starting point for structure-guided design of selective PKG Iα inhibitors.

## Experimental procedures

### *Expression and Purification of hPKG Iα C-domain*

The sequence encoding human PKG Iα C-domain (327-671) was cloned into pBlueBacHis2A vector. The vector was modified to put a tobacco etch virus (TEV) protease site just before the PKG coding sequence. The protein was expressed in High Five cells. The cells were grown at 28 °C and infected at an MOI of 3.0 for 32 h. All cells were lysed in Buffer A (25 mM Tris (pH 7.5), 500 mM NaCl, and 1 mM β-mercaptoethanol,) with Constant Systems TS cell disrupter (Daventry Northants, United Kingdom) and cleared via ultracentrifugation. The supernatant was loaded onto a Bio-Rad Nuvia nickel affinity column, washed with Buffer A and eluted with Buffer A containing 300 mM imidazole. His-tag was removed by incubating the sample with TEV protease at 4 °C overnight. TEV was removed from the protein sample by performing a second nickel affinity chromatography and collecting the flow-through fractions. The sample was further purified by anion exchange chromatography (Mono Q 10/100 GL, GE Healthcare) in Buffer B (25 mM Tris (pH 7.5), and 1 mM β-mercaptoethanol) with and without 1M Sodium Chloride. This was followed by size exclusion chromatography (Hiload 16/60 Superdex 75, GE Healthcare) in Buffer C (25 mM Tris (pH 7.5), 150 mM Sodium Chloride, and 1 mM tris(2-carboxyethyl)phosphine (TCEP).

### *Expression and Purification of hPKA Cα*

The pET15b plasmid encoding human PKA Cα was transformed into BL21 (DE3) *E. Coli* cells. The cells were grown at 37 °C until $OD_{600}$=1.0 was reached. The expression was induced by 0.5 mM isopropyl β-D-1-thiogalactopyranoside (IPTG) at 18 °C for 18 h. The cells were then lysed by the Constant Systems TS cell disruptor in Buffer A. The lysate was then cleared by ultracentrifugation and membrane filtration. The supernatant was applied onto a GE His-Trap column for nickel affinity purification. The protein was eluted by Buffer A containing 300 mM imidazole. The His-tag was removed by incubating the protein with TEV protease at 4 °C overnight followed by a second nickel affinity chromatography. The protein was then further purified by anion exchange chromatography (anion exchange chromatography, Mono Q 10/100 GL, GE Healthcare) in Buffer D (25 mM Potassium Phosphate (pH 7.0) and 1 mM β-mercaptoethanol) with and without 1 M Sodium Chloride. This was followed by size exclusion chromatography (Hiload 16/60 Superdex 75, GE Healthcare) in Buffer C.



Downloaded from http://www.jbc.org/ at University of California, Berkeley on November 28, 2018

***Crystallization and Structure Determination***

To obtain crystals of the PKG Iα C-domain:N46 complex, 14 mg $mL^{-1}$ of the PKG Iα C-domain was incubated with 1 mM of N46 for 30 min at room temperature. Crystals were obtained by mixing 1 µL of the C-domain:N46 complex solution with 1 µL of well solution (24% w/v PEG 1500 and 20% v/v glycerol) and 0.2 µL of additive (30% w/v trimethylamine N-oxide dyhydrate) at 22 °C. To obtain crystals of the PKA Cα:N46 complex, 12 mg $mL^{-1}$ of PKA Cα was incubated with 1 mM of N46 for 30 min at room temperature. Crystals were obtained by mixing 0.2 µL of the C-domain:N46 complex solution with 16% (w/v) PEG 8000, 0.04 M potassium phosphate (monobasic) and 20% (v/v) glycerol. PKG Iα C-domain and PKA Cα crystals were cryoprotected by paratone and diffraction images were collected at the Advanced Light Source (Berkeley, CA). Data were processed using CCP4.iMosflm (41). The structures of the PKG Iα C-domain:N46 and PKA Cα:N46 complexes were determined by Phaser-MR using AMP-PNP bound PKG Iα C-domain (PDB ID: 6BG2) and balanol-bound PKA Cα (PDB ID: 1BX6) as molecular replacement probes (42). Both structures were manually built using Coot and refined using Phenix.Refine (43,44). Figures were generated using PyMOL (Schrödinger, LLC)

***In Vitro Kinase Assays***

Flag-tagged wild-type and mutant PKG Iα proteins were purified from transiently transfected 293T cells as described (45). PKA Cα was purified as described above. The purified kinases were diluted in Kinase Dilution Buffer [10 mM potassium phosphate (pH 7.0), 1 mM EDTA, 35 mM β-mercaptoethanol, and 0.1% BSA] such that the reactions produced ~$10^5$ counts per reaction (corresponding to about 36 pmol phosphate incorporation). Reactions were initiated by adding 10µl diluted kinase to 5µl 3x kinase reaction mix [120 mM HEPES (pH 7.4), 1.56 mg/ml Kemptide, 30 mM $MgCl_2$, 300 µM ATP, 360 µCi/ml $^{32}$P-γ-ATP and 30 µM cGMP] containing variable amounts of the N46 inhibitor diluted in DMSO (control assays contained DMSO alone). Reactions were run for 1.5 min at 30 ºC and stopped by spotting on P81 phosphocellulose paper. Unincorporated $^{32}$P-γ-ATP was removed by washing P81 paper 4x 2 liters in 0.45% o-phosphoric acid. $^{32}$P incorporation was measured by liquid scintillation counting.

Downloaded from http://www.jbc.org/ at University of California, Berkeley on November 28, 2018

**Acknowledgments**

We thank Andrey Kovalevsky and Friedrich W. Herberg for critical reading of the manuscript. We also thank Paul Leonard (M.D. Anderson Cancer Center) for assistance in the initial screening of the PKG Iα:N46 complex crystals and Ying-Ju Sung (Geisinger Commonwealth School of Medicine) for kindly providing N46. C.K. was funded by the NIH grant R01 GM090161. D.E.C was funded by NIH Grant RO1 HL132141. This project was supported in part by the Protein and Monoclonal Antibody Production Shared Resource at Baylor College of Medicine with funding from NIH Cancer Center Support Grant P30 CA125123. The Berkeley Center for Structural Biology is supported in part by the National Institutes of Health, the National Institute of General Medical Sciences, and the Howard Hughes Medical Institute. The ALS-ENABLE beamlines are supported in part by the National Institutes of Health, National Institute of General Medical Sciences, grant P30 GM124169-01. The Advanced Light Source is a Department of Energy Office of Science User Facility under Contract No. DE-AC02-05CH11231. The Pilatus detector was funded under NIH grant S10OD021832.

**Conflict of interest**

The authors declare that they have no conflicts of interest with the contents of this article.

**Accession codes**

Coordinates and structural factors for PKG Iα C-domain and PKA Cα bound with N46 have been deposited at the RCSB Protein Data Bank with an accession codes, 6C0T and 6C0U, respectively.

**Author contributions**

L.Q. and C.K. conceived and designed the project. L.Q. optimized the expression conditions and purification protocols for the PKG Iα C-domain and PKA Cα. L.Q. purified the proteins used for

crystallization, obtained the co-crystals and solved their co-crystal structures. B.S. performed the diffraction experiments and data collection. D.E.C and S.A generated the wild-type and mutant PKG Iα expression constructs, made the mutant PKA Cα construct, and performed the kinase assays. L.Q., D.E.C., and C.K. wrote the manuscript and created the figures. All authors commented on the manuscript.

**Supporting Information**

Structural alignment of PKG Iα and PKA Cα bound with N46 (Figure S1), Crystal packing mediated by the N-terminal helix of the PKA Cα:N46 (Figure S2), Structural alignment between the PKG Iα C:N46 and PKA Cα:N46 complexes at their glycine rich loop (Figure S3), Comparison of interactions between PKA Cα and balanol or N46 (Figure S4), Structural alignment between PKG Iα C and PKCα (Figure S5), Sequence alignment between PKG Iα and PKA Cα (Figure S6), Data and refinement statistics (Table. S1).

Downloaded from http://www.jbc.org/ at University of California, Berkeley on November 28, 2018

**References**


1. Walitt, B., Nahin, R. L., Katz, R. S., Bergman, M. J., and Wolfe, F. (2015) The Prevalence and Characteristics of Fibromyalgia in the 2012 National Health Interview Survey. *PLoS One* **10**, e0138024
2. Services, U. S. D. o. H. H. (2016) Facing addiction in America: The Surgeon General's report on alcohol, drugs, and health.
3. Rummans, T. A., Burton, M. C., and Dawson, N. L. (2018) How Good Intentions Contributed to Bad Outcomes: The Opioid Crisis. *Mayo Clin Proc* **93**, 344-350
4. Advisors, T. C. o. E. (2017) The Underestimated Cost of the Opioid Crisis.
5. Ryan, S. A. (2018) Calculating the real costs of the opioid crisis. *Pediatrics* **141**, e20174129
6. Hedegaard, H., Warner, M., and Minino, A. M. (2017) Drug Overdose Deaths in the United States, 1999-2016.
7. Marsico, F., Paolillo, S., and Filardi, P. P. (2017) NSAIDs and cardiovascular risk. *J Cardiovasc Med (Hagerstown)* **18 Suppl 1: Special Issue on The State of the Art for the Practicing Cardiologist: The 2016 Conoscere E Curare Il Cuore (CCC) Proceedings from the CLI Foundation**, e40-e43
8. Arora, A., and Scholar, E. M. (2005) Role of tyrosine kinase inhibitors in cancer therapy. *J Pharmacol Exp Ther* **315**, 971-979
9. Koya, D., and King, G. L. (1998) Protein kinase C activation and the development of diabetic complications. *Diabetes* **47**, 859-866
10. Boric, M., Jelicic Kadic, A., and Puljak, L. (2014) Cutaneous expression of calcium/calmodulin-dependent protein kinase II in rats with type 1 and type 2 diabetes. *J Chem Neuroanat* **61-62**, 140-146
11. Fountas, A., Diamantopoulos, L. N., and Tsatsoulis, A. (2015) Tyrosine Kinase Inhibitors and Diabetes: A Novel Treatment Paradigm? *Trends Endocrinol Metab* **26**, 643-656
12. Tsuda, M., Mizokoshi, A., Shigemoto-Mogami, Y., Koizumi, S., and Inoue, K. (2004) Activation of p38 mitogen-activated protein kinase in spinal hyperactive microglia contributes to pain hypersensitivity following peripheral nerve injury. *Glia* **45**, 89-95
13. Milligan, E. D., and Watkins, L. R. (2009) Pathological and protective roles of glia in chronic pain. *Nat Rev Neurosci* **10**, 23-36
14. Berndt, N., Karim, R. M., and Schonbrunn, E. (2017) Advances of small molecule targeting of kinases. *Curr Opin Chem Biol* **39**, 126-132
15. Luo, C., Gangadharan, V., Bali, K. K., Xie, R. G., Agarwal, N., Kurejova, M., Tappe-Theodor, A., Tegeder, I., Feil, S., Lewin, G., Polgar, E., Todd, A. J., Schlossmann, J., Hofmann, F., Liu, D. L., Hu, S. J., Feil, R., Kuner, T., and Kuner, R. (2012) Presynaptically localized cyclic GMP-dependent protein kinase 1 is a key determinant of spinal synaptic potentiation and pain hypersensitivity. *PLoS Biol* **10**, e1001283
16. Sung, Y. J., Chiu, D. T., and Ambron, R. T. (2006) Activation and retrograde transport of protein kinase G in rat nociceptive neurons after nerve injury and inflammation. *Neuroscience* **141**, 697-709
17. Gangadharan, V., Wang, X., and Luo, C. (2017) [EXPRESS] Cyclic GMP-dependent protein kinase-I localized in nociceptors modulates nociceptive cortical neuronal activity and pain hypersensitivity. *Mol Pain* **13**, 1744806917701743
18. Sung, Y. J., Sofoluke, N., Nkamany, M., Deng, S., Xie, Y., Greenwood, J., Farid, R., Landry, D. W., and Ambron, R. T. (2017) A novel inhibitor of active protein kinase G attenuates chronic inflammatory and osteoarthritic pain. *Pain* **158**, 822-832
19. Hofmann, F., and Wegener, J. W. (2013) cGMP-Dependent Protein Kinases (cGK). in *Guanylate Cyclase and Cyclic GMP: Methods and Protocols* (Krieg, T., and Lukowski, R. eds.), Humana Press, Totowa, NJ. pp 17-50
20. Francis, S. H., Busch, J. L., Corbin, J. D., and Sibley, D. (2010) cGMP-dependent protein kinases and cGMP phosphodiesterases in nitric oxide and cGMP action. *Pharmacol Rev* **62**, 525-563


Downloaded from http://www.jbc.org/ at University of California, Berkeley on November 28, 2018

21. Alverdi, V., Mazon, H., Versluis, C., Hemrika, W., Esposito, G., van den Heuvel, R., Scholten, A., and Heck, A. J. (2008) cGMP-binding prepares PKG for substrate binding by disclosing the C-terminal domain. *J Mol Biol* **375**, 1380-1393
22. Wall, M. E., Francis, S. H., Corbin, J. D., Grimes, K., Richie-Jannetta, R., Kotera, J., Macdonald, B. A., Gibson, R. R., and Trewhella, J. (2003) Mechanisms associated with cGMP binding and activation of cGMP-dependent protein kinase. *Proc Natl Acad Sci U S A* **100**, 2380-2385
23. Butt, E. (2009) cGMP-Dependent Protein Kinase Modulators. in *cGMP: Generators, Effectors and Therapeutic Implications* (Schmidt, H. H. H. W., Hofmann, F., and Stasch, J.-P. eds.), Springer Berlin Heidelberg, Berlin, Heidelberg. pp 409-421
24. Wolfertstetter, S., Huettner, J. P., and Schlossmann, J. (2013) cGMP-Dependent Protein Kinase Inhibitors in Health and Disease. *Pharmaceuticals (Basel)* **6**, 269-286
25. Butt, E., van Bemmelen, M., Fischer, L., Walter, U., and Jastorff, B. (1990) Inhibition of cGMP-dependent protein kinase by (Rp)-guanosine 3',5'-monophosphorothioates. *FEBS letters* **263**, 47-50
26. Campbell, J. C., VanSchouwen, B., Lorenz, R., Sankaran, B., Herberg, F. W., Melacini, G., and Kim, C. (2016) Crystal structure of PKG Ibeta CNB-B:Rp-cGMPS complex reveals an apo-like, inactive conformation. *FEBS letters*
27. Engh, R. A., Girod, A., Kinzel, V., Huber, R., and Bossemeyer, D. (1996) Crystal structures of catalytic subunit of cAMP-dependent protein kinase in complex with isoquinolinesulfonyl protein kinase inhibitors H7, H8, and H89. Structural implications for selectivity. *J Biol Chem* **271**, 26157-26164
28. Gustafsson, A. B., and Brunton, L. L. (1999) Differential and selective inhibition of protein kinase A and protein kinase C in intact cells by balanol congeners. *Mol Pharmacol* **56**, 377-382
29. Ono-Saito, N., Niki, I., and Hidaka, H. (1999) H-series protein kinase inhibitors and potential clinical applications. *Pharmacol Ther* **82**, 123-131
30. Setyawan, J., Koide, K., Diller, T. C., Bunnage, M. E., Taylor, S. S., Nicolaou, K. C., and Brunton, L. L. (1999) Inhibition of protein kinases by balanol: specificity within the serine/threonine protein kinase subfamily. *Mol Pharmacol* **56**, 370-376
31. Koide, K., Bunnage, M. E., Gomez Paloma, L., Kanter, J. R., Taylor, S. S., Brunton, L. L., and Nicolaou, K. C. (1995) Molecular design and biological activity of potent and selective protein kinase inhibitors related to balanol. *Chem Biol* **2**, 601-608
32. Hidaka, H., and Kobayashi, R. (1992) Pharmacology of protein kinase inhibitors. *Annu Rev Pharmacol Toxicol* **32**, 377-397
33. Burkhardt, M., Glazova, M., Gambaryan, S., Vollkommer, T., Butt, E., Bader, B., Heermeier, K., Lincoln, T. M., Walter, U., and Palmetshofer, A. (2000) KT5823 inhibits cGMP-dependent protein kinase activity in vitro but not in intact human platelets and rat mesangial cells. *J Biol Chem* **275**, 33536-33541
34. Bain, J., McLauchlan, H., Elliott, M., and Cohen, P. (2003) The specificities of protein kinase inhibitors: an update. *Biochem J* **371**, 199-204
35. Narayana, N., Diller, T. C., Koide, K., Bunnage, M. E., Nicolaou, K. C., Brunton, L. L., Xuong, N. H., Ten Eyck, L. F., and Taylor, S. S. (1999) Crystal structure of the potent natural product inhibitor balanol in complex with the catalytic subunit of cAMP-dependent protein kinase. *Biochemistry* **38**, 2367-2376
36. Osborne, B., Wu, J., McFarland, C., NIckl, C., Sankaran, B., Casteel, D. E., Woods, V. J., Kornev, A., Taylor, S., and Dostmann, W. R. (2011) Crystal structure of cGMP-dependent protein kinase reveals novel site of interchain communication. *Structure* **19**, 1317-1327
37. Qin, L., Reger, A. S., Guo, E., Yang, M. P., Zwart, P., Casteel, D. E., and Kim, C. (2015) Structures of cGMP-Dependent Protein Kinase (PKG) Ialpha Leucine Zippers Reveal an Interchain Disulfide Bond Important for Dimer Stability. *Biochemistry* **54**, 4419-4422
38. Kim, J. J., Lorenz, R., Arold, S. T., Reger, A. S., Sankaran, B., Casteel, D. E., Herberg, F. W., and Kim, C. (2016) Crystal Structure of PKG I:cGMP Complex Reveals a cGMP-Mediated Dimeric Interface that Facilitates cGMP-Induced Activation. *Structure*


Downloaded from http://www.jbc.org/ at University of California, Berkeley on November 28, 2018

39. Campbell, J. C., Henning, P., Franz, E., Sankaran, B., Herberg, F. W., and Kim, C. (2017) Structural Basis of Analog Specificity in PKG I and II. *ACS Chem Biol* **12**, 2388-2398
40. Wagner, J. r., von Matt, P., Sedrani, R., Albert, R., Cooke, N., Ehrhardt, C., Geiser, M., Rummel, G., Stark, W., and Strauss, A. (2009) Discovery of 3-(1 H-Indol-3-yl)-4-[2-(4-methylpiperazin-1-yl) quinazolin-4-yl] pyrrole-2, 5-dione (AEB071), a Potent and Selective Inhibitor of Protein Kinase C Isotypes. *J Med Chem* **52**, 6193-6196
41. Battye, T. G., Kontogiannis, L., Johnson, O., Powell, H. R., and Leslie, A. G. (2011) iMOSFLM: a new graphical interface for diffraction-image processing with MOSFLM. *Acta Crystallogr D Biol Crystallogr* **67**, 271-281
42. McCoy, A. J., Grosse-Kunstleve, R. W., Adams, P. D., Winn, M. D., Storoni, L. C., and Read, R. J. (2007) Phaser crystallographic software. *J Appl Crystallogr* **40**, 658-674
43. Emsley, P., and Cowtan, K. (2004) Coot: model-building tools for molecular graphics. *Acta Crystallogr D Biol Crystallogr* **60**, 2126-2132
44. Afonine, P. V., Grosse-Kunstleve, R. W., Echols, N., Headd, J. J., Moriarty, N. W., Mustyakimov, M., Terwilliger, T. C., Urzhumtsev, A., Zwart, P. H., and Adams, P. D. (2012) Towards automated crystallographic structure refinement with phenix.refine. *Acta Crystallogr D Biol Crystallogr* **68**, 352-367
45. Kalyanaraman, H., Zhuang, S., Pilz, R. B., and Casteel, D. E. (2017) The activity of cGMP-dependent protein kinase Ialpha is not directly regulated by oxidation-induced disulfide formation at cysteine 43. *J Biol Chem* **292**, 8262-8268
46. Ho, B. K., and Gruswitz, F. (2008) HOLLOW: generating accurate representations of channel and interior surfaces in molecular structures. *BMC Struct Biol* **8**, 49


Downloaded from http://www.jbc.org/ at University of California, Berkeley on November 28, 2018

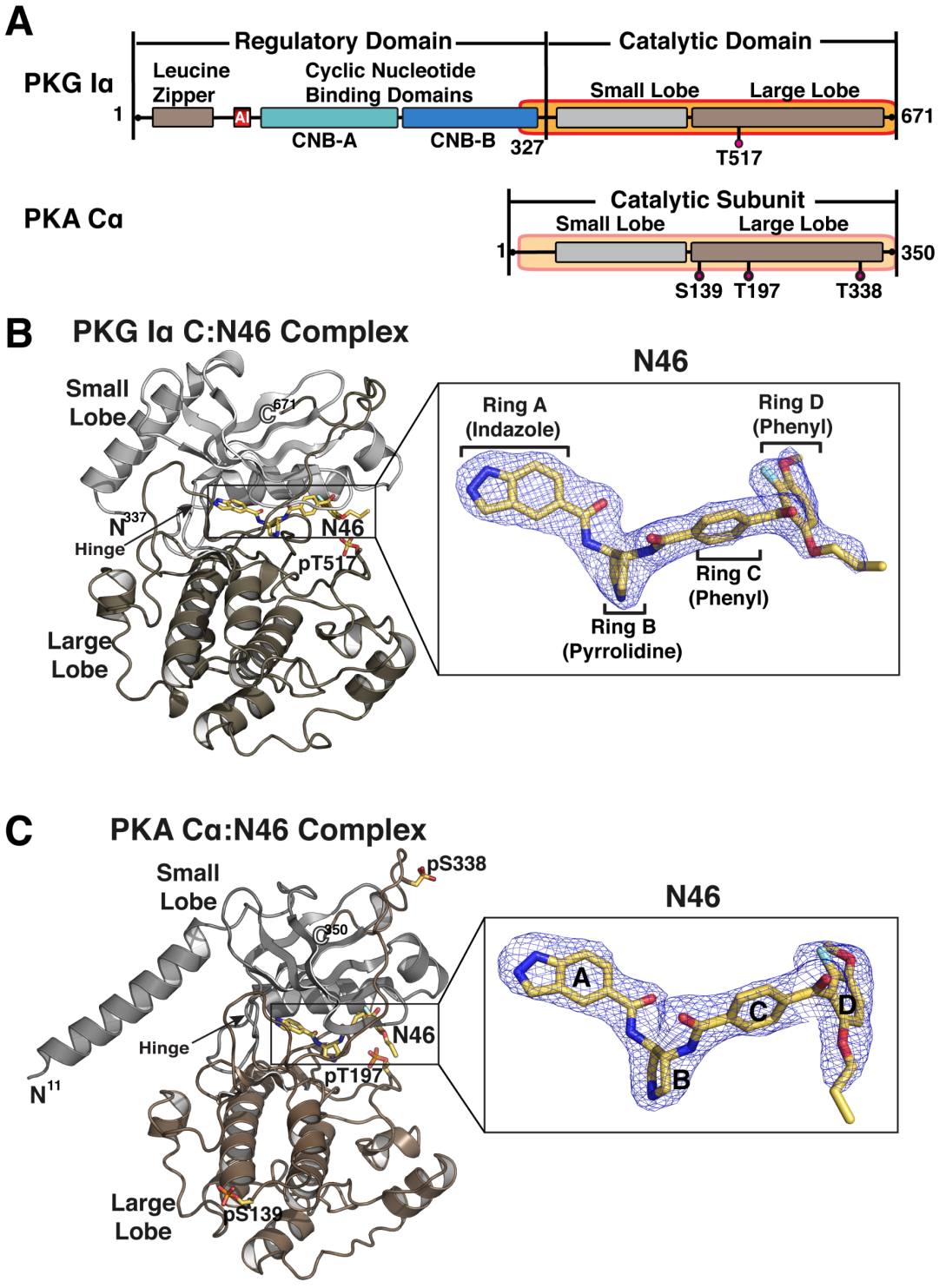


**Figure 1. Domain organizations and overall structures of N46 Bound PKG Iα and PKA Cα.** (A) The domain organizations of PKG Iα and PKA Cα. The catalytic domains used for crystallization are shaded in orange and labeled with the corresponding residue numbers. Phosphorylated residues are indicated (PKG Iα T517 and PKA Cα S139/T197/S338). Overall structures of the PKG Iα C:N46 (B) and PKA Cα:N46 (C) complexes. The N-and C-termini are labeled with corresponding residue numbers. The structures are rendered as *cartoon* with N46 shown as *sticks*. The small and large lobes are colored *gray* and *tan*, respectively. Atoms in N46 are colored as follows: carbons, *yellow*; oxygen, *red*; nitrogen, *blue;* fluorine, *cyan*. Zoom-in views show |*Fo-Fc*| omit maps of N46 (contoured at 3.0 σ level).



Downloaded from http://www.jbc.org/ at University of California, Berkeley on November 28, 2018

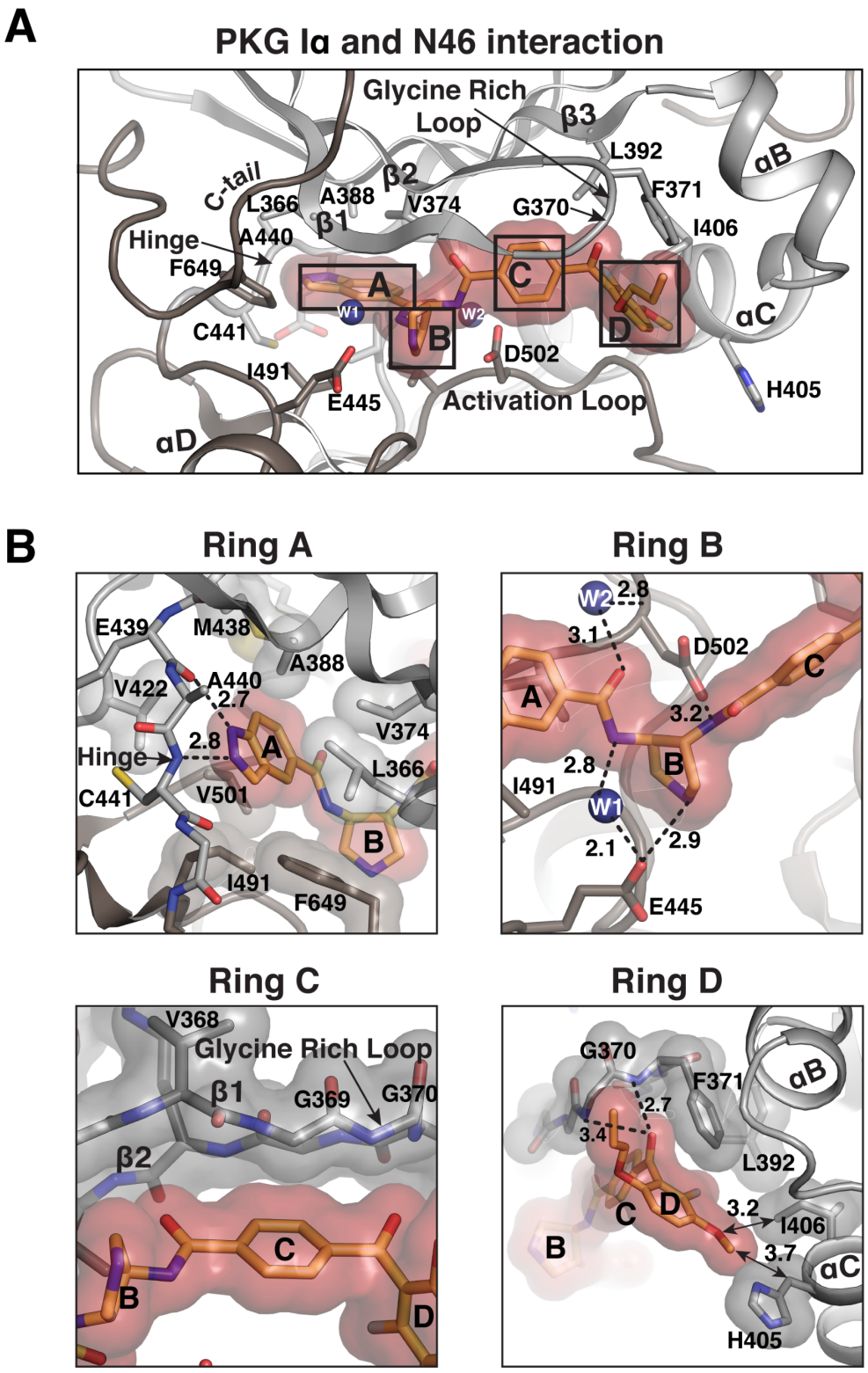


**Figure 2. Interactions between PKG Iα C-domain and N46.** (A) Detailed interactions with N46. Only the regions near the active site are shown. N46 is shown with *transparent surface.* Residues contacting N46 are shown as *sticks*. Water molecules are shown as *blue spheres*. (B) Zoomed-in views for each ring of N46, highlighting its interactions with different regions of the active site. Residues that provide VDW interactions are shown with *transparent surface.* Hydrogen bonds are shown as *dotted lines* and arrows indicate key VWD interactions with distances indicated in angstroms.



Downloaded from http://www.jbc.org/ at University of California, Berkeley on November 28, 2018

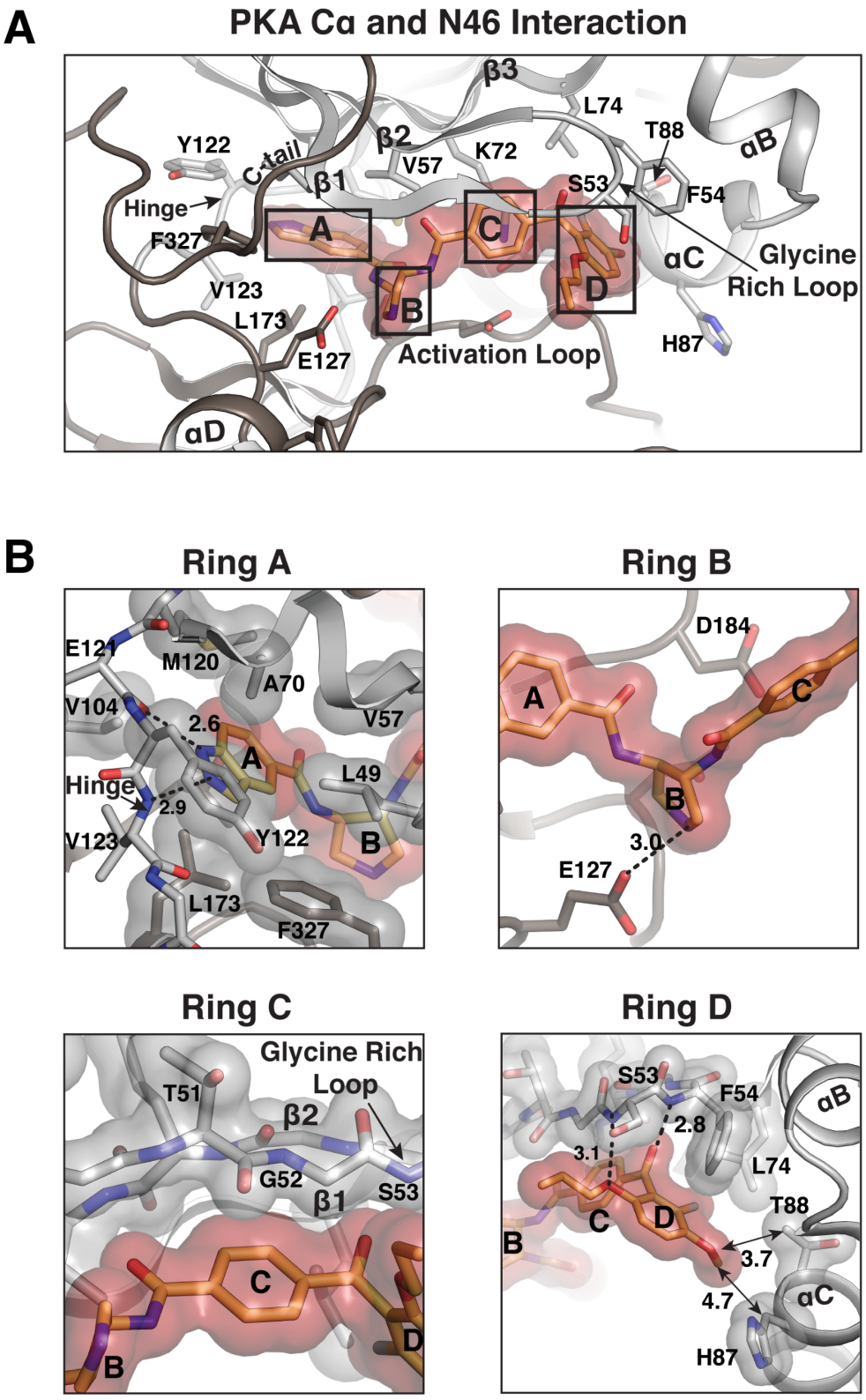


**Figure 3. Interactions between PKA Cα and N46.** (A) Detailed interactions with N46. Only the regions near the active site are shown. Residues contacting N46 are shown as *sticks*. (B) Zoomed-in views for each ring of N46, highlighting its interactions with different regions of the active site. Residues that provide VDW interactions are shown with *transparent surface.* Hydrogen bonds are shown as *dotted lines* with their distances given in angstroms.



Downloaded from http://www.jbc.org/ at University of California, Berkeley on November 28, 2018

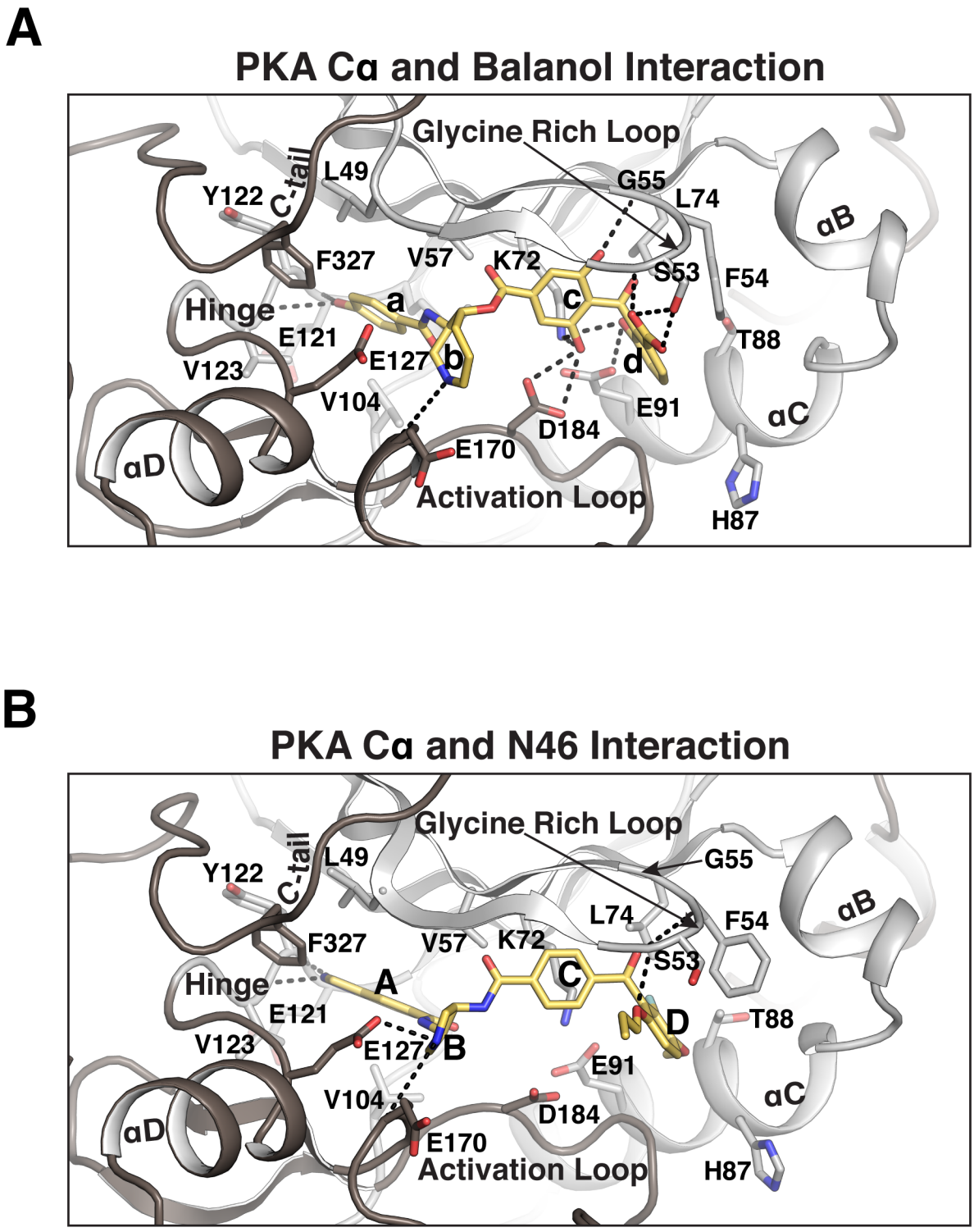


**Figure 4. Structural comparison between PKA Cα bound with balanol and N46.** Detailed interactions between PKA Cα and balanol (PDB ID, 1BX6) (A) orN46 (B). Only the regions near the active site are shown. Residues contacting balanol or N46 are shown as *sticks*. Direct hydrogen bonds are shown as *dotted lines*. The rings of balanol and N46 are labeled a-d and A-D, respectively.



Downloaded from http://www.jbc.org/ at University of California, Berkeley on November 28, 2018

**A**

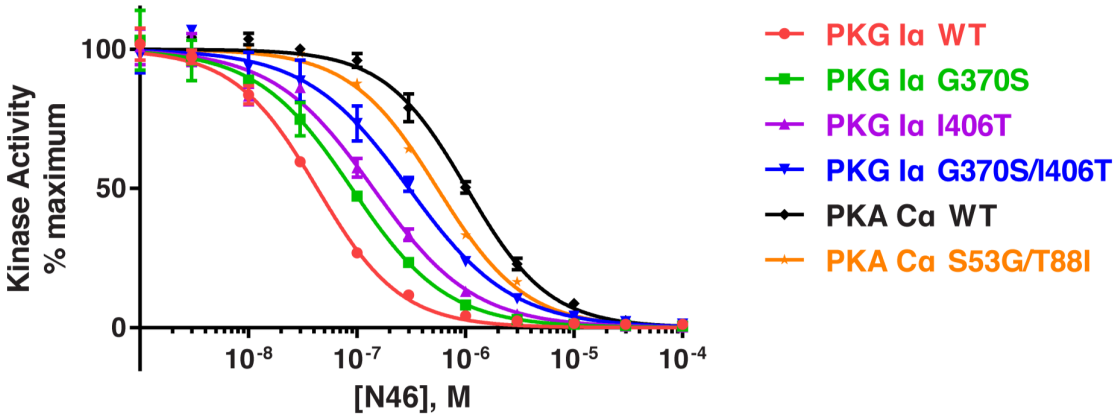


**B**

| Protein | $IC_{50}$, nM | Fold Change |
|---|---|---|
| PKG Iα WT | 43.1 ± 1.5 | 1.0 |
| PKG Iα G370S | 89.7 ± 5.4 | 2.1 |
| PKG Iα I406T | 141.5 ± 9.5 | 3.3 |
| PKG Iα G370S/I406T | 300.8 ± 18.6 | 7.0 |
| PKA Cα WT | 1030 ± 43 | 23.9 |
| PKA Cα S53G/T88I | 552.4 ± 18.3 | 12.8 |

**Figure 5. N46 inhibition of PKG Iα and PKA Cα.** (A) We performed *in vitro* kinase inhibition assays using purified wild-type and mutant PKG Iα and PKA Cα in the presence of increasing concentrations of N46, as described in Experimental Procedures. (B) Shows a table of $IC_{50}$ values based on the curves shown in A.

Downloaded from http://www.jbc.org/ at University of California, Berkeley on November 28, 2018

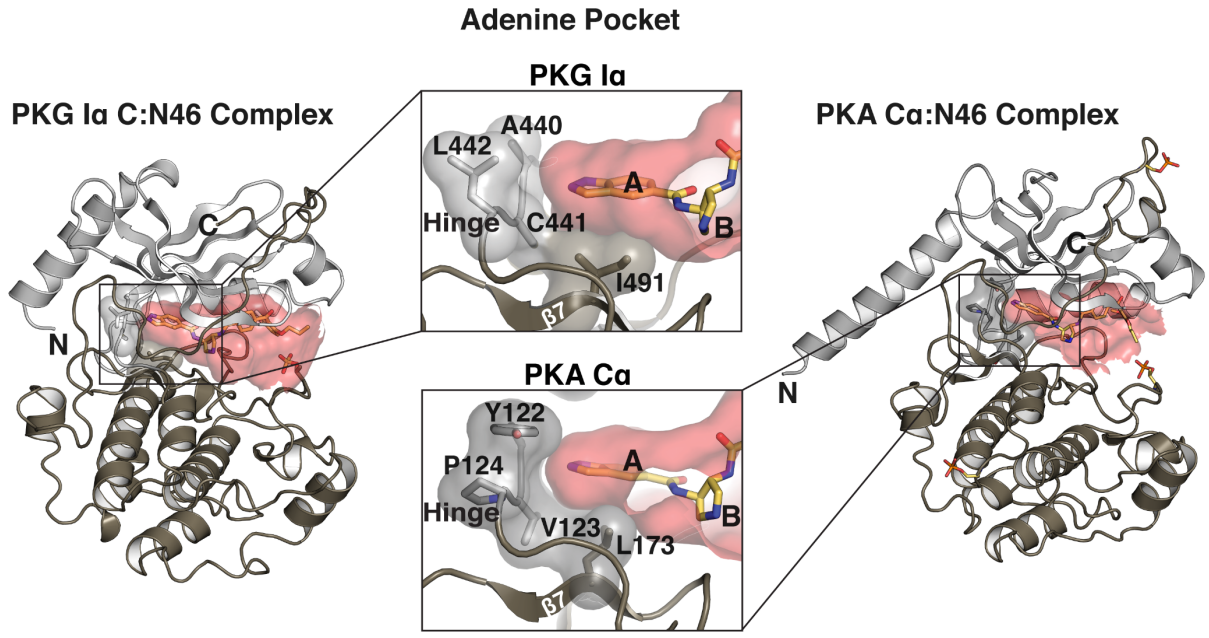


**Figure 6. Adenine Pockets of PKG and PKA.** The surfaces of the active site pockets for PKG Iα C-domain and PKA Cα are colored in red. Zoom-in views show the adenine pockets. The active site pockets are calculated using Hollow (46).

Downloaded from http://www.jbc.org/ at University of California, Berkeley on November 28, 2018

**Structural basis for selective inhibition of human PKG Iα by the balanol-like compound N46**

Liying Qin, Banumathi Sankaran, Sahar Aminzai, Darren Casteel and Choel Kim

*J. Biol. Chem. published online May 16, 2018*

---

Access the most updated version of this article at doi: 10.1074/jbc.RA118.002427

Alerts:
- When this article is cited
- When a correction for this article is posted

Click here to choose from all of JBC's e-mail alerts

Downloaded from http://www.jbc.org/ at University of California, Berkeley on November 28, 2018